A new Michaelis–Menten-based kinetic model for transport and phosphorylation of glucose and its analogs in skeletal muscle

Hsuan-Ming Huang
Department of Biomedical Engineering, Case Western Reserve University, Cleveland, Ohio 44106

Faramarz Ismail-Beigi
Department of Medicine, University Hospitals and Cleveland VA Medical Center, Case Western Reserve University, Cleveland, Ohio 44106

Raymond F. Muzic, Jr.[a)]
Department of Radiology, University Hospitals Case Medical Center, Case Western Reserve University, Cleveland, Ohio 44106

(Received 21 January 2011; revised 8 April 2011; accepted for publication 20 May 2011; published 25 July 2011)

Purpose: A new model is introduced that individually resolves the delivery, transport, and phosphorylation steps of metabolism of glucose and its analogs in skeletal muscle by interpreting dynamic positron emission tomography (PET) data.
Methods: The model uniquely utilizes information obtained from the competition between glucose and its radiolabeled analogs. Importantly, the model avoids use of a lumped constant which may depend on physiological state. Four basic physiologic quantities constitute our model parameters, including the fraction of total tissue space occupied by interstitial space (f_{IS}), a flow-extraction product and interstitial (IS_g) and intracellular (IC_g) glucose concentrations. Using the values of these parameters, cellular influx (CI) and efflux (CE) of glucose, glucose phosphorylation rate (PR), and maximal transport (V^G) and phosphorylation capacities (V^H) can all be determined. Herein, the theoretical derivation of our model is addressed and characterizes its properties via simulation. Specifically, the model performance is evaluated by simulation of basal and euglycemic hyperinsulinemic (EH) conditions.
Results: In fitting the model-generated, synthetic data (including noise), mean estimates of all but IC_g of the parameter values are within 5% of their values for both conditions. In addition, mean errors of CI, PR, and V^G are less than 5% whereas those of V^H and CE are not.
Conclusions: It is concluded that under the conditions tested, the novel model can provide accurate parameter estimates and physiological quantities, except IC_g and two quantities that are dependent on IC_g, namely CE and V^H. However, the ability to estimate IC_g seems to improve with increases in intracellular glucose concentrations as evidenced by comparing IC_g estimates under basal vs EH conditions. [DOI: 10.1118/1.3599034]

Key words: glucose transport, radiopharmaceutical, PET, glucose clamp

I. INTRODUCTION

In positron emission tomography (PET), the glucose analog labeled with the radionuclide ^{18}F, 2-fluoro-2-deoxy-D-glucose ([^{18}F]2FDG), is widely used to study glucose metabolism, especially in brain. It is well known that the uptake of glucose and its analogs, such as [^{18}F]2FDG, from plasma to brain utilize glucose transporters, primarily GLUT1, to cross the blood-brain barrier. Once inside the cell, [^{18}F]2FDG is phosphorylated by hexokinase forming [^{18}F]FDG-6-phosphate, which is trapped intracellularly. To probe these processes, two-compartment models with three (3K model) and four (4K model) rate constants were proposed by Sokoloff *et al.*[1] and Phelps *et al.*,[2] respectively. Both models lump extracellular and intracellular glucose into a single compartment and therefore cannot resolve the transport step.

Herein, our emphasis is on glucose handling by skeletal muscle which, because of its overall mass, is one of the largest consumers of glucose in the body and is the target of some pharmaceuticals used to treat diabetes. The application of the above-mentioned 3K and 4K models to skeletal muscle is controversial.[3] Unlike brain, skeletal muscle does not have a tight barrier between capillary and interstitial space. In skeletal muscle, glucose diffuses into interstitial space from plasma through pores and fenestrations between endothelial cells in capillaries. Glucose then enters cells via facilitative glucose transporters, GLUT1 and GLUT4, with GLUT4 being dominant in mediating the glucose transport response to insulin. Once inside the cell, glucose phosphorylation is catalyzed by hexokinase. Since the 3K and 4K models lump extracellular and intracellular glucose into the same compartment, these models cannot independently account for glucose transport from plasma into cells. Consequently, a three-compartment five-rate-constant model (5K model) was proposed by Bertoldo *et al.*[3] that resolves glucose metabolism into three individual steps: delivery, transport, and

phosphorylation. While the level of detail is an important advantage of this 5K model, it is challenging to reliably determine values for all of the model's parameters.

To this end, Bertoldo and co-workers have used sequential injections of the nonphosphorylatable glucose analog ^{11}C-labeled 3-O-methyl-D-glucose [^{11}C]3OMG) and the phosphorylatable analog [^{18}F]2FDG to obtain more information than can be obtained with only a single injection.[4] They endeavored to more reliably resolve the transport and phosphorylation steps. This approach seems appropriate, yet challenges remain: First, [^{11}C]3OMG, a reference tracer for glucose transport in PET has a limitation in its clinical use due to the 20-min half-life of ^{11}C. Second, a value for a lumped constant (LC) must be assumed so that one may infer the glucose metabolic rate from that of the analog, whereas the value depends on plasma and tissue glucose concentrations.[5,6] Third, the 5K model[3] has five parameters (i.e., five rate constants), which make their reliable estimation difficult. Fourth, no direct estimation of the interstitial and intracellular glucose concentrations is provided by this 5K or any other published PET glucose model.

Herein, we address these challenges. We use a nonphosphorylatable analog ^{18}F-labeled 6-fluoro-6-deoxy-D-glucose [^{18}F]6FDG), which has a 110-min half-life and has been shown to be transported but not phosphorylated.[7] We propose a novel model that resolves delivery, transport, and phosphorylation steps and which explicitly accounts for interactions between glucose and its analog thereby obviating the need for a lumped constant. Our proposed model incorporates physiologic constraints and well-established kinetic laws and requires four independent parameters to be estimated from the PET data.

We first introduce the theoretical derivation of our model and present studies characterizing its ability to estimate parameter values in computer simulations wherein the estimates can be compared to the known true values. We then design a two-injection protocol for PET scanning. The experimental procedure utilizes PET scanning upon injection of [^{18}F]6FDG followed by a subsequent injection of [^{18}F]2FDG with continued scanning. This two-injection simulation protocol is performed for both basal (fasting) and euglycemic hyperinsulinemic (EH) conditions.

II. METHODS AND MATERIALS

II.A. Kinetic modeling of glucose analogs in skeletal muscle

Similar to the 5K model, our model has three compartments with five rate constants. Molar concentrations of the glucose analog in the arterial plasma, interstitial, and intracellular spaces are denoted P_a, IS_a, and IC_a, respectively, and the intracellular concentration of the phosphorylated analog denoted IP_a is assumed to be metabolically trapped inside the cell. In this model, total tissue space (V_{total}) is the sum of interstitial (V_{IS}), intracellular (V_{IC}), and blood (V_b) spaces. From the molar balance, the following equations define the quantitative relationship for the kinetic model:

$$V_{IS}\frac{d}{dt}IS_a(t) = FE[P_a(t) - IS_a(t)] - k_{3a}V_{IS}IS_a(t) + k_{4a}V_{IC}IC_a(t), \quad (1)$$

$$V_{IC}\frac{d}{dt}IC_a(t) = k_{3a}V_{IS}IS_a(t) - k_{4a}V_{IC}IC_a(t) - k_{5a}V_{IC}IC_a(t), \quad (2)$$

$$V_{IC}\frac{d}{dt}IP_a(t) = k_{5a}V_{IC}IC_a(t). \quad (3)$$

Based on the assumptions that the interstitial space is a well-mixed compartment and that capillaries in the tissue are uniformly distributed, Johnson and Wilson[8] showed that when the intracapillary solute concentrations equilibrate rapidly compared with the interstitial solute concentrations, the flow-extraction product (FE, ml/min) can be used to describe the transcapillary flux of solutes from plasma to interstitial space. In addition, Renkin[9] showed that when solutes cross the capillary wall primarily by diffusion, the first term of the right side of Eq. (1), i.e., $FE[P_a(t)\text{-}IS_a(t)]$, can be used to quantify the exchange of solutes, e.g., glucose analogs, between plasma and interstitial space. The rate constants k_{3a} and k_{4a} denote transport of glucose analogs by glucose transporters. Inside the cell, the rate constant k_{5a} describes the phosphorylation of glucose analogs catalyzed by hexokinase.

Now, we can normalize Eqs. (1)–(3) by total tissue space (V_{total}).

$$f_{IS}\frac{d}{dt}IS_a(t) = k_1P_a(t) - k_2f_{IS}IS_a(t) - k_{3a}f_{IS}IS_a(t) + k_{4a}f_{IC}IC_a(t), \quad (4)$$

$$f_{IC}\frac{d}{dt}IC_a(t) = k_{3a}f_{IS}IS_a(t) - k_{4a}f_{IC}IC_a(t) - k_{5a}f_{IC}IC_a(t), \quad (5)$$

$$f_{IC}\frac{d}{dt}IP_a(t) = k_{5a}f_{IC}IC_a(t), \quad (6)$$

where $f_{IS} = V_{IS}/V_{total}$, $f_{IC} = V_{IC}/V_{total}$, $k_1 = FE/V_{total}$, and $k_2 = k_1/f_{IS}$. Herein, we assume that glucose and its analogs have the same rate constant $k_1 (= FE/V_{total})$ because they are carried by blood flow (F) and have similar extraction (E). Since we define $k_2 = k_1/f_{IS}$, the rate constant k_2 is the same for glucose and its analogs. To derive the final model equations for parameter estimates, we define $IS'_a(t) = f_{IS}IS_a(t)$, $IC'_a(t) = f_{IC}IC_a(t)$, and $IP'_a(t) = f_{IC}IP_a(t)$. As a result, Eqs. (4)–(6) can be written as

$$\frac{d}{dt}IS'_a(t) = k_1P_a(t) - k_2IS'_a(t) - k_{3a}IS'_a(t) + k_{4a}IC'_a(t), \quad (7)$$

$$\frac{d}{dt}IC'_a(t) = k_{3a}IS'_a(t) - k_{4a}IC'_a(t) - k_{5a}IC'_a(t), \quad (8)$$

$$\frac{d}{dt}IP'_a(t) = k_{5a}IC'_a(t). \quad (9)$$

Now, as shown in Fig. 1, our model can be described by Eqs. (7)–(9), which are the final model equations used for parameter estimates.

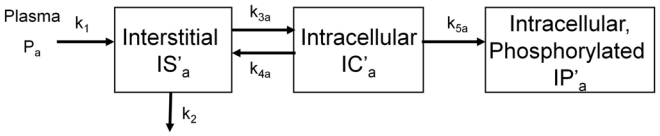

FIG. 1. Kinetic model for glucose analogs.

PET images pixel values are calibrated to the total radioactivity concentration, which is calculated by multiplying molar concentration by specific activity and summing activities in all compartments:

$$C_{PET,i} = \frac{1}{t_e^i - t_b^i}\int_{t_b^i}^{t_e^i}\{A[IS'_a(t) + IC'_a(t) + IP'_a(t)] + f_b \times B(t)\}dt. \quad (10)$$

where B(t) is the decay-corrected whole blood activity, and f_b ($=V_b/V_{total}$) is the fraction of total tissue space occupied by blood space. Integration over time and division by frame duration yields the time-averaged value between the beginning t_b^i and ending time t_e^i of frame i. A is the specific activity in units of activity per quantity (μCi/pmol). According to Eqs. (7)–(10), six model parameters are k_1, f_{IS}, k_{3a}, k_{4a}, k_{5a}, and f_b. In Sec. II B, we would show that the rate constants k_{3a}, k_{4a}, and k_{5a} can be expressed in terms of k_1, f_{IS}, IS_g, and IC_g and that the final model parameters to be estimated are k_1, f_{IS}, IS_g, and IC_g.

II.B. Classic Michaelis–Menten kinetics

Using classic enzyme-substrate kinetics, a glucose analog is modeled as a competitive inhibitor of glucose transport and phosphorylation. Consequently, the reaction velocity V_a, of either process, for substrate (glucose analog) at concentration S_a can be expressed as $V_a = V_{max} \times (S_a/K_a)/[1+S_a/K_a+S_g/K_g]$, where V_{max} is the maximum velocity, K_a is the Michaelis constant for the analog, K_g is the Michaelis constant for glucose, and S_g is the concentration of glucose.[10] Generally speaking, the concentration of radiolabeled glucose analog in a PET study is much less than its Michaelis constant so that S_a/K_a is small compared to one and may be neglected in the denominator. With this simplification, substituting the appropriate interstitial or intracellular concentration for substrate concentration S_a into this velocity expression, and dividing by S_a, we obtain the effective rate "constants" k_{3a} and k_{4a} for transport and k_{5a} for phosphorylation of the glucose analog

$$k_{3a} = \frac{V_a^G}{f_{IS}(K_a^G + IS_g K_a^G/K_g^G)}, \quad (11)$$

$$k_{4a} = \frac{V_a^G}{f_{IC}(K_a^G + IC_g K_a^G/K_g^G)}, \quad (12)$$

$$k_{5a} = \frac{V_a^H}{f_{IC}(K_a^H + IC_g K_a^H/K_g^H)}. \quad (13)$$

We use the symbols V to denote maximum velocities in units of millimole per minute per milliliter tissue and K to denote Michaelis constants. Superscripts G and H denote glucose transporter and hexokinase, respectively. Subscripts a and g denote glucose analog and glucose, respectively. IS_g, (millimole per milliliter interstitial space) and IC_g (millimole per milliliter intracellular space) are, respectively, the interstitial and intracellular concentrations of glucose. Based on the assumption that glucose transport is bidirectional and symmetric, Michaelis constants for the forward and reverse transport are equal[11] and the units of K_a^G and K_g^G are millimoles per mililiter of distribution volume, which are interstitial and intracellular spaces for influx and efflux, respectively. In the right side of Eq. (11), the units in the numerator are millimoles per minute per milliliter tissue, the units within the parentheses in the denominator are millimoles per mililiter interstitial space, and the unit of f_{IS} in the denominator is milliliter interstitial space per milliliter tissue so that k_{3a} has the expected units of per minute. Analogously, in the right sides of Eqs. (12) and (13) the units in the numerators are millimoles per minute per milliliter tissue, the units in the parentheses of the denominators are millimoles per milliliter intracellular space, and f_{IC} has units of milliliter intracellular space per milliliter tissue so that k_{4a} and k_{5a} have units of per minute. Note that the rate constant k_{5a} is only pertinent to glucose or its analogs that can be phosphorylated. From Eqs. (11)–(13), it is clear that values of k_{3a}, k_{4a}, and k_{5a} depend on IS_g and IC_g and thus are not actually constants. However, if PET studies are performed when glucose concentrations are stable, k_{3a}, k_{4a}, and k_{5a} may be treated as constants during the studies. Michaelis constants for glucose and its analogs are assumed to be fixed values under most physiological conditions and will be determined separately via transporter assays. Now, given assumed Michaelis constants (i.e., K_a^G, K_a^H, K_g^G, and K_g^H), model parameters are k_1, f_{IS}, f_{IC}, f_b, V_a^G, V_a^H, IS_g, and IC_g. As detailed below, physiologic constraints are applied so that the final model parameters are k_1, f_{IS}, IS_g, and IC_g.

PET studies are performed with steady glucose concentrations. Accordingly, the left sides of differential equations for glucose—analogous to Eqs. (4) and (5) with replacement of subscripts a by g in all symbols to denote glucose—equate to zero and the differential equations simplify to algebraic equations

$$f_{IS}\frac{d}{dt}IS_g(t) = 0 = k_1[P_g - IS_g] - k_{3g}f_{IS}IS_g + k_{4g}f_{IC}IC_g, \quad (14)$$

$$f_{IC}\frac{d}{dt}IC_g(t) = 0 = k_{3g}f_{IS}IS_g - k_{4g}f_{IC}IC_g - k_{5g}f_{IC}IC_g, \quad (15)$$

In addition, plasma (P_g), interstitial (IS_g), and intracellular (IC_g) glucose concentrations are assumed to be constant over the time-course of PET studies. The rate constant expressions k_{3g}, k_{4g}, and k_{5g} for glucose are obtained from those of its analog Eqs. (11)–(13) by replacing the values of maximum velocities and Michaelis constants of the analog with those of glucose. Thus, rate constant k_{3g}, k_{4g}, and k_{5g} can be written as

$$k_{3g} = \frac{V_g^G}{f_{IS}(K_g^G + IS_g)}, \quad (16)$$

$$k_{4g} = \frac{V_g^G}{f_{IC}(K_g^G + IC_g)}, \quad (17)$$

$$k_{5g} = \frac{V_g^H}{f_{IC}(K_g^H + IC_g)}. \quad (18)$$

After substituting Eqs. (16)–(18) into the steady-state equations for glucose Eqs. (14) and (15), one has

$$k_1(P_g - IS_g) - \frac{V_g^G}{(K_g^G + IS_g)} IS_g + \frac{V_g^G}{(K_g^G + IC_g)} IC_g = 0, \quad (19)$$

$$\frac{V_g^G}{(K_g^G + IS_g)} IS_g - \frac{V_g^G}{(K_g^G + IC_g)} IC_g - \frac{V_g^H}{(K_g^H + IC_g)} IC_g = 0. \quad (20)$$

Solving Eq. (19) for V_g^G, one has

$$V_g^G = \frac{k_1(P_g - IS_g)}{[IS_g/(K_g^G + IS_g) - IC_g/(K_g^G + IC_g)]}. \quad (21)$$

According to Eq. (19), we know that $k_1(P_g\text{-}IS_g) = V_g^G\, IS_g/(K_g^G + IS_g)\text{-}V_g^G\, IC_g/(K_g^G + IC_g)$ and then Eq. (20) can be written as

$$k_1(P_g - IS_g) - \frac{V_g^H}{(K_g^H + IC_g)} IC_g = 0. \quad (22)$$

Solving Eq. (22) for V_g^H, one has

$$V_g^H = \frac{k_1(P_g - IS_g)}{IC_g/(K_g^H + IC_g)}. \quad (23)$$

Since glucose and its analogs have similar molecular weights and chemical properties and are acted upon by the same transporter, we assume that $V_a^G = V_g^G$ as have others for GLUT1.[12–14] We assume the case to be analogous for GLUT4. Thus, for simplicity, we denote V_a^G and V_g^G as V^G. The analogous assumption, i.e. $V_a^H = V_g^H$, is applied for hexokinase so we, likewise, denote V_a^H and V_g^H by V^H. After substituting Eqs. (21) and (23) into Eqs. (11)–(13), the rate constants k_{3a}, k_{4a}, and k_{5a} are

$$k_{3a} = \frac{1}{f_{IS}(K_a^G + IS_g K_a^G/K_g^G)} \times \frac{k_1(P_g - IS_g)}{[IS_g/(K_g^G + IS_g) - IC_g/(K_g^G + IC_g)]}, \quad (24)$$

$$k_{4a} = \frac{1}{f_{IC}(K_a^G + IC_g K_a^G/K_g^G)} \times \frac{k_1(P_g - IS_g)}{[IS_g/(K_g^G + IS_g) - IC_g/(K_g^G + IC_g)]}, \quad (25)$$

$$k_{5a} = \frac{1}{f_{IC}(K_a^H + IC_g K_a^H/K_g^H)} \times \frac{k_1(P_g - IS_g)}{IC_g/(K_g^H + IC_g)}. \quad (26)$$

Since blood space (V_b) in skeletal muscle is relatively small as compared to V_{IS} and V_{IC},[15] we assume that $V_{total} \approx V_{IS} + V_{IC}$. As a result, $f_{IC} = V_{IC}/V_{total} \approx 1\text{-}f_{IS}$, for skeletal muscle. Thus, given measured P_g and assumed Michaelis constants, the rate constants k_{3a}, k_{4a}, and k_{5a} can be expressed in terms of k_1,f_{IS},IS_g, and IC_g. The assumption also indicates that $f_b \times B(t)$ in Eq. (10) may be ignored. At the end of Sec. II A, six parameters to be estimated are k_1, f_{IS}, k_{3a}, k_{4a}, k_{5a}, and f_b. With these simplifications, the final model parameters are k_1, f_{IS}, IS_g, and IC_g. These are *a priori* locally identifiable (see Appendix A).[16]

II.C. Classic Simulations of PET data in rat skeletal muscle

PET simulations were performed using COMKAT.[17,18] Using Eq. (10), synthetic data without including radioactive decay were generated with a plasma input (P_a) function defined as

$$P_a(t) = (A_1 t - A_2 - A_3)e^{-L_1 t} + A_2 e^{-L_2 t} + A_3 e^{-L_3 t}. \quad (27)$$

with $A_1 = 800$, $A_2 = 3$, $A_3 = 2$ pmol/ml; $L_1 = 20$, $L_2 = 0.6$, and $L_3 = 0.01$ min^{-1} for 6FDG and $A_1 = 1500$, $A_2 = 24$, $A_3 = 6$ pmol/ml; $L_1 = 16$, $L_2 = 1.2$, and $L_3 = 0.03$ min^{-1} for 2FDG under basal conditions.[19] (Note that in [^{18}F]2FDG and [^{18}F]6FDG prepared for PET studies, the amount of labeled analog is negligible as compared to amount of unlabeled 2FDG and 6FDG, respectively.) In practice, EH conditions would have lower concentration of 2FDG (or 6FDG) in plasma than basal conditions because the muscular uptake of glucose and its analog is increased by insulin. Thus, we increase the values of L_1, L_2, and L_3 of 2FDG and 6FDG by 25% for EH conditions.

Based on the published data,[3,15] the fraction of the total tissue space occupied by the blood space ($f_b = V_b/V_{total}$) is negligible in rat skeletal muscle. Thus, we assume that skeletal muscle has 75% intracellular space (f_{IC}), 25% interstitial space (f_{IS}) and neglect f_b. The value of the Michaelis constant for glucose transport K_g^G is set to 3.5 mM (Ref. 20) and that of phosphorylation by hexokinase K_g^H is set to 0.13 mM.[21] As the Michaelis constant for 6FDG transport (K_{6FDG}^G) has not yet been determined, we made a preliminary estimate of 10 mM based on published[22] and unpublished experimental data. Also, we assume that the Michaelis constant of 2FDG transport (K_{2FDG}^G) is 8 mM based on unpublished experimental data and that of phosphorylation by hexokinase K_{2FDG}^H equals 0.17 mM.[21]

For both basal and EH conditions, plasma glucose concentration (P_g) was set to 6 mM, consistent with our prior experimental data in the rat.[22] IS_g was specified as 85% of P_g (=5.1 mM) and 50% of P_g (=3 mM) for basal and EH conditions, respectively.[19] From the skeletal muscle blood flow in rats,[23] we assume $k_1 = 0.04$ min^{-1} for basal conditions. In rat skeletal muscle, fasting intracellular free glucose concentration (IC_g) is close to zero[20] so that IC_g is set to 0.05 mM for basal conditions. Given these values, we solved Eqs. (21) and (23) to obtain values of V^G (=0.06 mmol/min/ml tissue) and V^H (=0.13 mmol/min/ml tissue). For EH conditions, wherein insulin brings transporters to the plasma membrane and stimulates phosphorylation, we increased the number of transporters (V^G) 5-fold[24] and hexokinase activity (V^H) 2-fold[25] and set $IS_g = 3$ mM. Given these values, we solved Eqs. (21) and (23) to obtain values for k_1 and IC_g. Interestingly, this indicates a 1.1-fold increase in k_1. Physiologically, this could be interpreted as an increase in blood flow.[26,27] Table I is the summary of values of parameters used for both conditions.

TABLE I. Summary of parameters used in basal and EH conditions.

Symbol	Description	Value for basal conditions	Value for EH conditions	Unit
k_1	Rate constant of diffusion of glucose and its analogs from plasma to interstitial space	0.040	0.044	ml/ml per min
IS_g	Interstitial glucose concentration	5.1	3.0	mmol/ml IS space
IC_g	Intracellular glucose concentration	0.050	0.135	mmol/ml IC space
V^G	Maximal transport capacity	0.06	0.31	mmol/min/ml tissue
V^H	Maximal phosphorylation capacity	0.13	0.26	mmol/min/ml tissue
K_g^G	Michaelis constant for glucose transport by GLUT4	3.5	3.5	mM
K_{2FDG}^G	Michaelis constant for 2FDG transport by GLUT4	8	8	mM
K_{6FDG}^G	Michaelis constant for 6FDG transport by GLUT4	10	10	mM
K_g^H	Michaelis constant for phosphorylation of glucose	0.13	0.13	mM
K_{2FDG}^H	Michaelis constant for phosphorylation of 2FDG	0.17	0.17	mM
CI	Cellular influx	0.0369	0.1435	mmol/min/ml tissue
CE	Cellular efflux	0.0009	0.0115	mmol/min/ml tissue
PR	Phosphorylation rate	0.0360	0.1320	mmol/min/ml tissue

With parameter values assigned above, we generated model output and treated it as simulated, noiseless PET data. To this we added simulated noise according to

$$\hat{D}_i = D_i + N(0, \sigma_i^2), \tag{28}$$

where $\hat{D}_i$ and D_i are, respectively, the noisy and the noiseless data at the ith frame. $N(0, \sigma_i^2)$ indicates deviates from a normal distribution with zero mean and variance σ_i^2. Standard deviation (SD) was set as

$$\sigma_i = \alpha[D_i/(t_e^i - t_b^i)]^{0.5}, \tag{29}$$

where α is the noise level.[28] Parameter values were estimated by minimizing the weighted least squares objective function

$$O_{WLS}(p) = \frac{1}{2}\sum_{i=1}^{n} w_i[C_{PET,i}(p) - \hat{D}_i]^2, \tag{30}$$

where p is the parameter vector (k_1, f_{IS}, IS_g, and IC_g), w_i is the weight for frame i, and $C_{PET,i}$ is the model output in frame i. In this simulation, we used the known SD to determine the weights w_i ($= 1/\sigma_i^2$) for fitting data. With the experimental data, we would use either the iteratively reweighted least squares or extended least squares methods to estimate the noise and to determine weights.[28] The data-fitting algorithm was performed with COMKAT's fit function that currently uses MATLAB 2010 b (The Mathworks, Inc., Natick, MA) function ''lsqcurvefit,'' a trust-region-reflective method.[29] In addition, data from both injections were considered as a single large set that was fit contemporaneously. In particular, model output [i.e., Eq. (10)] was calculated by summing the radioactivity from the two radiopharmaceuticals. We repeated this minimization 500 times producing 500 sets of parameter estimates, one set for each of 500 simulated, noisy data sets. This entire process was performed twice: during basal and EH conditions. For both basal and EH conditions, initial guesses for k_1, IS_g, IC_g, and f_{IS} were 0.1 min^{-1}, 4.0 mM, 0.1 mM, and 0.15, and the bounds were set as $0.001 \le k_1 \le 0.5$ min^{-1}, $2 \le IS_g \le 6$ mM, $0.001 \le IC_g \le 0.5$ mM and $0.1 \le f_{IS} \le 0.5$. Means and standard deviations (SD) of the parameter estimates were calculated from estimates obtained by fitting the 500 data sets. Also, bias and precision were summarized using mean ±SD of estimation errors [estimation error = (estimated value − true value)/true value × 100%]. Cellular influx (CI), efflux (CE), and phosphorylation rate (PR) of glucose can be determined as

$$CI = f_{IS} \times k_{3g} \times IS_g = V^G \times IS_g/(K_g^G + IS_g), \tag{31}$$

$$CE = f_{IC} \times k_{4g} \times IC_g = V^G \times IC_g/(K_g^G + IC_g), \tag{32}$$

$$PR = f_{IC} \times k_{5g} \times IC_g = V^H \times IC_g/(K_g^H + IC_g), \tag{33}$$

In skeletal muscle, upon cellular entry glucose is phosphorylated by hexokinase and further metabolized. Since muscle lacks glucose-6-phosphatase, glucose-6-phosphate cannot be dephosphorylated and exit the cells. Consequently, PR is equal to glucose metabolic rate,[30] the usual outcome measurement of the 3K and 4K models used with [^{18}F]2FDG data.

The simulated experimental protocol included a 1-h PET scan beginning with a bolus injection of [^{18}F]6FDG (t = 0 min) and then continued with another hour of PET scanning after a bolus injection of [^{18}F]2FDG at t = 60 min. As a result, the total simulated imaging time of this two-injection protocol was fixed to 2 h. To emulate the time-sampling inherent with PET we binned the data into a sequence of 2-s (n = 6) frames followed by sequences of 6-s (n = 8), 15-s (n = 16), 60-s (n = 5) and finally 300-s (n = 10) frames. To visualize parameter estimates in terms of bias and precision, we use box plots. A gray bar shows the central 50 percentile and the horizontal black line within the box designates the median. Circles indicate outliers defined as estimates that are below the lower quartile or above the upper quartile by more than 1.5 times the difference between the upper and lower quartile.

III. RESULTS

III.A. Model behaviors under basal and EH conditions

Noise-free time-activity curves (TACs) under both conditions are shown in Fig. 2. As compared to basal conditions, EH conditions cause an increase in the later tissue radioactivity for [^{18}F]6FDG, which is consistent with our previous

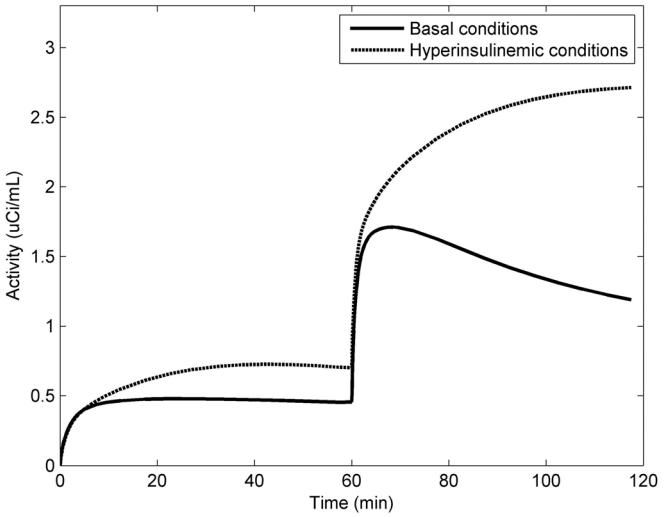

FIG. 2. Noise-free tissue TACs after injecting a bolus of [^{18}F]6FDG and [^{18}F]2FDG at 0 and 60 min, respectively, under basal and EH conditions.

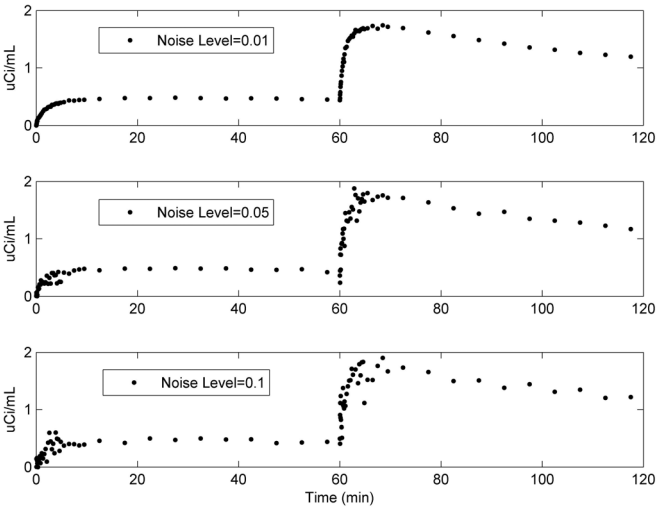

FIG. 4. Model-predicted [^{18}F]6FDG (i.e., 0–60 min) and [^{18}F]2FDG (i.e., 60–120 min) time-activity curves during basal conditions at noise levels of 0.01, 0.05, and 0.1.

[^{18}F]6FDG studies.[22] For [^{18}F]2FDG, the later tissue radioactivity increases with time under EH conditions, but decreases under basal conditions. To explain the different curve shapes of these two conditions, we plot the model-predicted radioactivity for each compartment in Fig. 3. In contrast to basal conditions, EH conditions have lower interstitial [^{18}F]6FDG (IS_{6FDG}) but higher intracellular [^{18}F]6FDG (IC_{6FDG}), which is attributed to an insulin-stimulated increase in the number of glucose transporters. Thus, EH conditions show higher tissue radioactivities for [^{18}F]6FDG. Also, similar effects are observed for [^{18}F]2FDG. But the difference is greater since once [^{18}F]2FDG enters the cell, it is rapidly phosphorylated. Upon entry, intracellular [^{18}F]2FDG (IC_{2FDG}) is immediately phosphorylated into [^{18}F]2FDG-6-P ($IP_{2FDG\text{-}6\text{-}P}$) by hexokinase and trapped inside cells. This causes rapid accumulation of $IP_{2FDG\text{-}6\text{-}P}$ under EH conditions compared to basal conditions, as expected. As a result, the tissue radioactivities after the injection of [^{18}F]2FDG keeps increasing under EH conditions, but promptly decreases under basal conditions.

With corresponding parameters specified above, we determined CI, CE, and PR of glucose under basal and EH conditions, Table I. At the basal state, CI is almost the same with PR but CE is much lower than CI and PR indicating that virtually all the glucose that enters the cell is phosphorylated and then further metabolized. In the insulin-stimulated state, the increases over basal conditions are CI: 0.1435, CE: 0.0115, and PR: 0.1320 mmol/min/ml tissue. This shows that synthetic data set exhibits reasonable physiologic behavior: at the basal state, the transport step is rate-limiting and hexokinase phosphorylates glucose essentially as fast as it is transported into cells whereas with insulin stimulation the phosphorylation step becomes more rate-determining.[31,32]

III.B. Summary of model fits and parameter estimates

Figure 4 shows TACs at different noise levels ($\alpha = 0.01$, 0.05, and 0.1) under basal conditions. The noise level $\alpha = 0.05$ best agreed with our prior experimental data (see

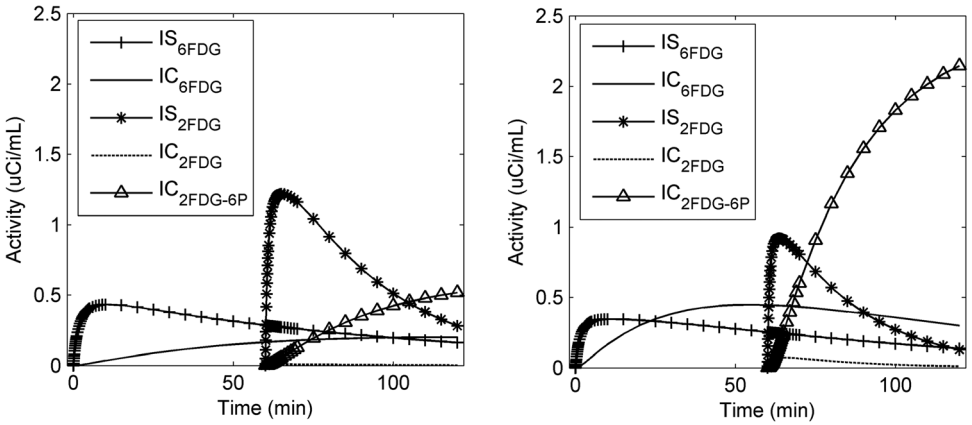

FIG. 3. Resolution of tissue radioactivities in each of three compartments after injection a bolus of [^{18}F]6FDG and [^{18}F]2FDG at 0 and 60 min, respectively, under basal (left) and EH (right) conditions.

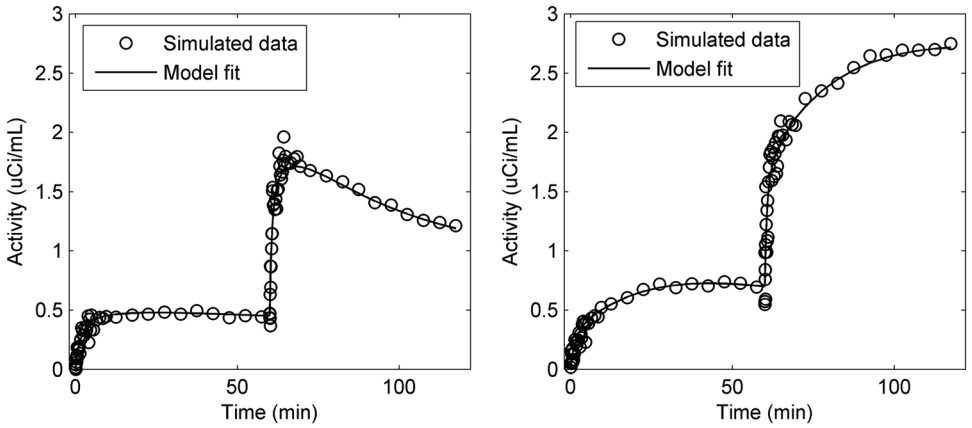

FIG. 5. Simulation data set (noise levels = 0.05) and model fit during basal (left) and EH (right) conditions.

Appendix B).[22] Example fits (noise level $\alpha = 0.05$) are shown in Fig. 5 for basal (left) and EH (right) conditions. Our model appears to fit the synthetic data well for both conditions noting the expected high variability in the data in early frames due to their short duration. In particular, the model parameters can generally be estimated. When the noise level $\alpha = 0.05$ was used for simulations, the results showed that in both basal and EH conditions, mean errors (i.e., biases) of the parameter values were $\leq 5\%$ with SD (i.e., precision) $<10\%$ for k_1, IS_g, f_{IS}, V^G, CI, and PR. However, under basal conditions, IC_g ($163 \pm 322\%$), CE ($159 \pm 312\%$) and V^H ($271 \pm 757\%$) show poor estimates (mean errors $\pm$ SD). Except V^H: $645 \pm 1559\%$, the other two parameters were better determined in the EH condition, IC_g: $37 \pm 115\%$ and CE: $41 \pm 119\%$, than in the basal condition.

To investigate the identifiability of each model parameter, the sensitivity functions, which are derivatives of model output with respect to the change of each parameter, for basal and EH conditions were evaluated in Fig. 6. In terms of curve shape, the sensitivity functions are different for different parameters. For a given parameter, the curve shapes are similar both in basal and EH conditions. From the magnitude, the value of the sensitivity function for IC_g is much less than that of the other parameters, which indicates that the data are relatively insensitive to IC_g. Thus, the estimates of IC_g with high bias and low precision are not surprising.

The distributions of parameter estimates of 500 trials obtained from both conditions at different noise levels ($\alpha = 0.01$, 0.05, and 0.1) were shown graphically in box plots, Fig. 7. Means and standard deviations of model parameters and individual rate constants for basal and EH conditions are tabulated in Tables SI and SII (see Appendix C), respectively. In addition, the summary of bias and precision of all parameters (Table SIII) for both basal and EH conditions is included in Appendix C. As noise levels are decreased, parameter estimates improve, especially for IC_g, CE, and V^H. For EH conditions, the number of outliers for V^H decreases as the noise level reduces to 0.01. For basal conditions, the box plot of V^H shows many outliers at each noise level, but PR which relates to V^H shows good precision with few outliers. At the highest noise level, the bias of IC_g, CE, and V^H exceeds 100% of its true value, but other parameters are estimated with a bias of less than 6%, indicating much less sensitivity to noise.

IV. DISCUSSION

IV.A. Model properties

Because of our physiologic-based assumptions, our model has fewer independent parameters that need to be estimated compared to other PET models that are used to assess glucose kinetics. Unique features of our model are that interstitial and intracellular glucose concentrations can be estimated directly and that the model does not use a lumped constant to relate kinetics of glucose to that of its labeled analog. We thereby avoid vagaries of using a possibly incorrect value of the lumped constant which might depend on dietary state,

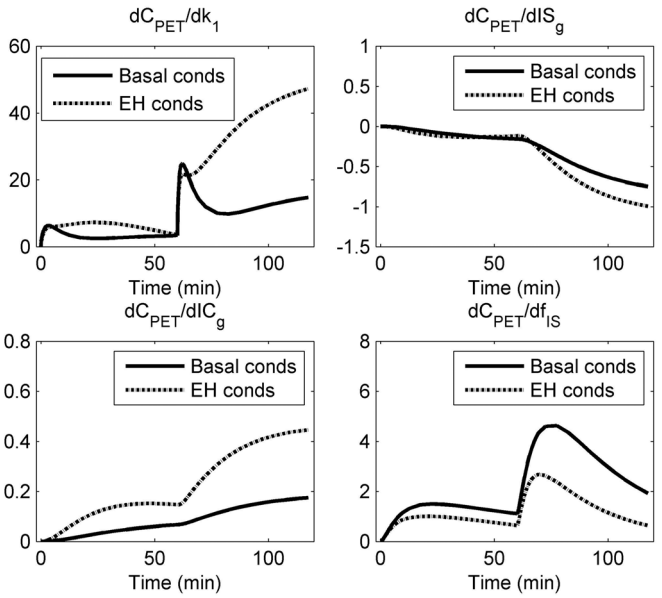

FIG. 6. Sensitivity functions under basal and hyperinsulinemic conditions. For both conditions, the magnitude of $dC_{PET}/(dIC_g)$ is low. This means that IC_g is insensitive to measured data.

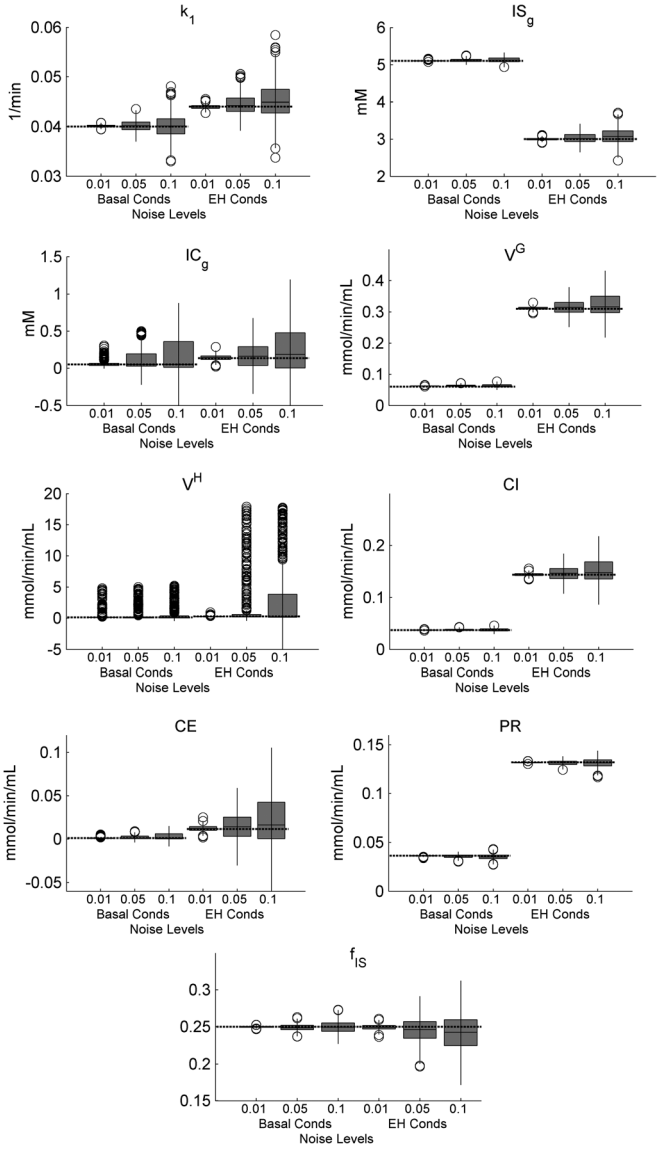

FIG. 7. The distribution of the parameter estimates is summarized by box plots for different noise levels ($\alpha = 0.01$, 0.05, and 0.1) under EH conditions. The gray bars denote the central 50 percentile, the black lines denote the median, the circles denote outliers, and the horizontal dashed lines denote the true values. The parameter estimates are well-behaved in that they converge toward the true value with diminishing noise level.

hormonal changes, and specifics of the tissue.[5,6] However, in this study, we have difficulties in estimates of IC_g and its related quantities: CE and V^H. In addition, the proposed model requires *a priori* knowledge of five Michaelis constants (see Table I) which can be determined experimentally by *in vitro* assays. When the values of Michaelis constants derived from *in vitro* assays are used for *in vivo* studies, we may consider the effect of *in vivo* versus *in vitro* values on parameter estimates.

Our proposed model estimates transport and phosphorylation rates of glucose, and offers a direct way to quantify the rates of the individual steps of glucose metabolism *in vivo*. Because the method could be applied to human experiments, it can provide details about glucose metabolism on a regional or organ level in ways that heretofore have not been available. Consequently, our model could potentially provide unique insight to the evolution of diabetes, insulin resistance, and treatment of such diseases.

IV.B. Model prediction

The novel model presented herein predicts responses of glucose and its analogs under various conditions. Since [^{18}F]6FDG is not phosphorylated, *a priori*, we expected insulin stimulation to impact the rate at which it achieves steady state between interstitial and intracellular spaces but not to impact the steady state concentration. Importantly, the model offers a mechanistic explanation for the increase of tissue radioactivity during EH conditions that was observed with nonphosphorylated analogs both in our own prior data[21] using [^{18}F]6FDG and those of Bertoldo *et al.*[4] using [^{11}C]3OMG. It is well known that insulin increases the number of functional GLUT4 transporters at the plasma membrane. The capacity for glucose to enter the cell may then exceed the phosphorylation rate while the intracellular concentration increases sufficiently until mass-action increases the phosphorylation rate to balance the influx.[33,34] The increased intracellular glucose concentration increases transport competition between glucose and its radiolabeled analog for cellular efflux. Under the increased transport competition, the efflux of intracellular radiolabeled analog decreases so that tissue radioactivity increases during EH conditions.

IV.C. Parameter estimates and limitations

In comparing all parameters, both conditions have relatively poor precision and high bias in estimates of IC_g, CE, and V^H. This may be an intrinsic limitation as physiologically IC_g is too low to provide measurable competition with the analog for efflux. However, the increase of IC_g from 0.05 to 0.135 mM (from basal to EH conditions) reduces mean errors from 163 to 37%. This indicates that our model would be able to obtain more accurate estimate for higher IC_g. In addition, the expected improvements of parameter estimates with decreases in noise levels are evident in Fig. 7. This behavior provides evidence that the software code is being implemented correctly.

Unlike other PET models, our model does not require a LC and therefore avoids the potential for incorrect values of the LC which depends on dietary state. However, our model requires Michaelis constants of glucose and its analogs. These constants can be determined experimentally in transporter assays. Based on our analysis (see Appendix B), for example, 20% bias in K_g^G slightly increases bias for IS_g, (by 3 and 9% for basal and EH conditions, respectively) but has no significant effect on k_1 and f_{IS}. Incorrect values for Michaelis constants have no effect on IC_g, which has high bias and low precision estimates.

IV.D. Application of the new model

Insulin resistance manifested as impaired glucose transport in response to insulin is one of the hallmarks of type 2 diabetes and obesity.[35] To assess insulin sensitivity,

hyperinsulinemic euglycemic glucose clamp methodology has been widely used in clinical studies.[36] However, this method indicates total body insulin sensitivity;[37] no regional or tissue-specific information is provided. Fortunately, some earlier studies[37,38] showed that the potential of dynamic *in vivo* PET imaging combined with kinetic models could provide valuable information about impaired glucose metabolism in skeletal muscle. In type 2 diabetic patients, many studies[35,39] showed that the impairment of glucose phosphorylation was greater than that of glucose transport under euglycemic hyperinsulinemic glucose clamp; hence, IC_g would be higher than in normal subjects. In this case, our model would perform even better than predicted herein because the poor precision was attributed to low IC_g. Further studies are needed to investigate the performance of our model in conditions of impaired glucose metabolism vs normal controls.

In addition to its use in characterizing glucose transport in striated muscle by GLUT4 and GLUT1, our model could be extended to evaluate renal (or intestinal) handling of glucose, which is transported into the cells by sodium-glucose cotransporters (SGLTs). Glucose transport in the kidney is a two-step process with SGLTs facilitating the first step at the luminal surface of proximal tubular cells and GLUT2 facilitating the second at the basolateral surface. For this, our model would be modified to include an additional transport step. This would be particularly promising with 6FDG because it is well-transported by both GLUTs and SGLTs.[7]

V. CONCLUSIONS

We have proposed and mathematically demonstrated local identifiability properties of a new model for describing transport and phosphorylation of glucose and its analogs in skeletal muscle. Except for intracellular glucose concentration, parameter estimates generally appear to be very accurate (unbiased) under various conditions. Unlike other PET models, our model has fewer model parameters to be estimated and obviates the use of lumped constant. Another unique feature of our model is that it provides direct estimates of interstitial and intracellular glucose concentrations (IS_g and IC_g, respectively, in the model). Moreover, we simulate the effect of insulin action by increasing maximal velocities for glucose transport and phosphorylation (i.e., V^G and V^H). In our model, this causes increases in cellular influx and efflux of glucose and glucose phosphorylation rate. These changes are consistent with the known physiological response to insulin stimulation. With these results, we expect that conditions associated with impaired glucose transport and abnormal glucose metabolism can be detected and evaluated by our model.

ACKNOWLEDGMENTS

This work was supported by National Institute of Diabetes and Digestive and Kidney Diseases Grant No.: R01 DK082423 (PIs: Muzic and Ismail-Beigi). The authors thank Dr. Chandramouli for discussion on our proposed method.

APPENDIX A: IDENTIFIABILITY ANALYSIS

To analyze a priori identifiability of the final model parameters using the transfer function method,[40] we start with the model equations shown in Eqs. (7)–(9).

$$\frac{d\,IS'_a(t)}{dt} = k_1 P_a(t) - k_2 IS'_a(t) - k_{3a} IS'_a(t) + k_{4a} IC'_a(t) \tag{A1}$$

$$\frac{d\,IC'_a(t)}{dt} = k_{3a} IS'_a(t) - k_{4a} IC'_a(t) - k_{5a} IC'_a(t) \tag{A2}$$

$$\frac{dIP'_a(t)}{dt} = k_{5a} IC'_a(t) \tag{A3}$$

In addition, the model output can be written as:

$$C_{PET}(t) = IS'_a(t) + IC'_a(t) + IP'_a(t) + f_b \times B(t) \tag{A4}$$

By taking Laplace transform of Eqs. (Al)–(A3), one has

$$sIS'_a(s) = k_1 P_a(s) - k_2 IS'_a(s) - k_{3a} IS'_a(s) + k_{4a} IC'_a(s) \tag{A5}$$

$$sIC'_a(s) = k_{3a} IS'_a(s) - k_{4a} IC'_a(s) - k_{5a} IC'_a(s) \tag{A6}$$

$$sIP'_a(s) = k_{5a} IC'_a(s) \tag{A7}$$

Solving for $IS'_a(s)$, $IC'_a(s)$ and $IS'_a(s)$ one has

$$IS'_a(s) = k_1 \frac{s + k_{4a} + k_{5a}}{(s + k_2 + k_{3a})(s + k_{4a} + k_{5a}) - k_{3a}k_{4a}} P_a(s) \tag{A8}$$

$$IC'_a(s) = k_1 \frac{k_{3a}}{(s + k_2 + k_{3a})(s + k_{4a} + k_{5a}) - k_{3a}k_{4a}} P_a(s) \tag{A9}$$

$$IP'_a(s) = k_1 \frac{k_{3a}k_{5a}}{s[(s + k_2 + k_{3a})(s + k_{4a} + k_{5a}) - k_{3a}k_{4a}]} P_a(s) \tag{A10}$$

Thus, the Laplace transform of $C_{PET}(t)$ can be written as

$$C_{PET}(s) = k_1 \frac{s^2 + s(k_{3a} + k_{4a} + k_{5a}) + k_{3a}k_{5a}}{s^3 + s^2(k_2 + k_{3a} + k_{4a} + k_{5a}) + s(k_2k_{4a} + k_2k_{5a} + k_{3a}k_{5a})} P_a(s) + f_b \times B(s) \tag{A11}$$

As a result, the six known observational parameters are

$$\Phi_1 = k_1 \tag{A12}$$

$$\Phi_2 = k_1(k_{3a} + k_{4a} + k_{5a}) \tag{A13}$$

$$\Phi_3 = k_1 k_{3a} k_{5a} \tag{A14}$$

$$\Phi_4 = k_2 + k_{3a} + k_{4a} + k_{5a} \tag{A15}$$

$$\Phi_5 = k_2k_{4a} + k_2k_{5a} + k_{3a}k_{5a} \tag{A16}$$

$$\Phi_6 = f_6 \tag{A17}$$

Thus, these six observational parameters are a priori uniquely identifiable. To assess the identifiability of the model parameters k_1, k_2, k_{3a}, k_{4a}, k_{5a} and f_b, we solve for them in terms of the observational parameters

$$k_1 = \Phi_1 \tag{A18}$$

$$k_2 = \frac{\Phi_1\Phi_4 - \Phi_2}{\Phi_1} \tag{A19}$$

$$k_{3a} = \frac{\Phi_2(\Phi_1\Phi_4 - \Phi_2) - \Phi_1(\Phi_1\Phi_5 - \Phi_3)}{\Phi_1(\Phi_1\Phi_4 - \Phi_2)} \tag{A20}$$

$$k_{4a} = \frac{\Phi_1\Phi_5 - \Phi_3}{\Phi_1\Phi_4 - \Phi_2} - \frac{\Phi_3(\Phi_1\Phi_4 - \Phi_2)}{\Phi_2(\Phi_1\Phi_4 - \Phi_2) - \Phi_1(\Phi_1\Phi_5 - \Phi_3)} \tag{A21}$$

$$k_{5a} = \frac{\Phi_3(\Phi_1\Phi_4 - \Phi_2)}{\Phi_2(\Phi_1\Phi_4 - \Phi_2) - \Phi_1(\Phi_1\Phi_5 - \Phi_3)} \tag{A22}$$

$$f_b = \Phi_6 \tag{A23}$$

The unique solutions indicate these six parameters are a priori uniquely identifiable. To test whether f_{IS}, f_{IC}, IS_g and IC_g are a priori uniquely identifiable, we solve for these in terms of the observational parameters. For f_{IS}, we substitute $k_2 = k_1/f_{IS}$, into Eq. (A19) to obtain

$$f_{IS} = \frac{\Phi_1\Phi_1}{\Phi_1\Phi_4 - \Phi_2} \tag{A24}$$

indicating it is a priori uniquely identifiable. The analyses for k_1, f_{IS}, f_{IC}, IS_g, and IC_g are more complex. As we described in Sec. II B, given known Michaelis constants and P_g, the rate constants k_{3a}, k_{4a} and k_{5a} can expressed in terms of k_1, f_{IS}, f_{IC}, IS_g, and IC_g,

$$k_{3a} = \frac{1}{f_{IS}(K_a^G + IS_gK_a^G/K_g^G)} \times \frac{k_1(P_g - IS_g)}{[IS_g/(K_g^G + IS_g) - IC_g/(K_g^G + IC_g)]} \tag{A25}$$

$$k_{4a} = \frac{1}{f_{IC}(K_a^G + IC_gK_a^G/K_g^G)} \times \frac{k_1(P_g - IS_g)}{[IS_g/(K_g^G + IS_g) - IC_g/(K_g^G + IC_g)]} \tag{A26}$$

$$k_{5a} = \frac{1}{f_{IC}(K_a^H + IC_gK_a^H/K_g^H)} \times \frac{k_1(P_g - IS_g)}{IC_g/(K_g^H + IC_g)]} \tag{A27}$$

Substituting Eqs. (A25)–(A27) into Eqs. (A20)–(A22), we can solve for f_{IC}, IS_g and IC_g in terms of known parameters, P_g, K_a^G, K_a^H, K_g^G, K_g^H, Φ_1, Φ_2, Φ_3, Φ_4 and Φ_5.

$$IS_g = \frac{-b \pm \sqrt{b^2 - 4ac}}{2a}$$

$$a = \frac{k_{3a}k_{5a}f_{IS}K_a^H}{k_1k_{4a}K_g^H} + \frac{k_{3a}f_{IS}K_a^G}{k_1K_g^G} + \left(\frac{k_{3a}k_{5a}f_{IS}K_a^H}{k_1k_{4a}K_g^H}\right)\left(\frac{k_{3a}f_{IS}K_a^G}{k_1K_g^G}\right)$$

$$b = (K_g^G - P_g)\left[\frac{k_{3a}k_{5a}f_{IS}K_a^H}{k_1k_{4a}K_g^H} + \frac{k_{3a}f_{IS}K_a^G}{k_1K_g^G}\right] + K_g^G\left(\frac{k_{3a}k_{5a}f_{IS}K_a^H}{k_1k_{4a}K_g^H}\right)\left(\frac{k_{3a}f_{IS}K_a^G}{k_1K_g^G}\right)$$

$$c = -P_gK_g^G\left(\frac{k_{3a}k_{5a}f_{IS}K_a^H}{k_1k_{4a}K_g^H} + \frac{k_{3a}f_{IS}K_a^G}{k_1K_g^G}\right) \tag{A28}$$

$$IC_g = \frac{K_g^G(P_g - IS_g)}{(k_{3a}k_{5a}f_{IS}K_a^H)(K_g^K + IS_g)/(k_1k_{4a}K_g^H) - P_g + IS_g} \tag{A29}$$

$$f_{IC} = f_{IS}\frac{k_{3a}(1 + IS_g/K_g^G)}{k_{4a}(1 + IC_g/K_g^G)} \tag{A30}$$

According to Eq. (A28), since $b^2 - 4ac \geq 0$, IS_g may have two real solutions. This shows the model, in terms of our final parameterization, can have at most two solutions. Accordingly, all six model parameters, k_1, f_{IS}, f_{IC}, f_b, IS_g and IC_g are a priori locally identifiable.

The identifiability of the proposed model derived above is for a phosphorylated glucose analog (i.e., 2FDG). For a non-phosphorylated glucose analog (i.e., 6FDG), we still have six model parameters, k_1 f_{IS}, f_{IC}, f_b, IS_g and IC_g. The Laplace transform of $C_{PET}(t)$ can be simply obtained by setting the rate constant k_{5a} of Eq. (A11) to zero. As a result, there are five known observational parameters and six unknown model parameters, indicating that these six model parameters are non-identifiable. However, since we assume for skeletal muscle $f_b + f_{IS} + f_{IC} = 1$ (i.e., $f_{IC} = 1 - f_{IS} - f_b$), the number of unknown model parameters is reduced from six to five. Again, we can solve for IS_g and IC_g in terms of known parameters, P_g, K_a^G, K_g^G and five observational parameters. Analogously, IS_g may have two real solutions. Accordingly, all five model parameters, k_1, f_{IS}, f_b, IS_g and IC_g are a priori locally identifiable.

In the case of a two-injection study, as we propose, which uses 6FDG followed by 2FDG, the information content of the combined data set is at least as great as that obtained with either 2FDG or 6FDG used alone. Consequently, the two-injection study is a priori locally identifiable.[40]

APPENDIX B: ANALYSIS OF NOISE LEVELS

In the figure shown below, we compare the tissue time-activity curves (TACs) for rat skeletal muscle during

[^{18}F]6FDG PET scans obtained from a preliminary study to those from the simulation. We observe that the noise level (α=0.05) used in simulation is in the range of that obtained from animal studies. To quantitatively estimate the noise level (a), we fit the noisy TAC ($\widehat{D}_i$, shown below) using the 5K model and treat the model fit as noise-free data (D_i). Then, the noise level would be estimated by calculating the standard deviation of $(\widehat{D}_i - D_i)/[D_i/(t_e^i - t_b^i)]^{0.5}$. As a result, the estimated noise level is 0.03 which shows that the value of $\alpha = 0.05$ might be a bit pessimistic indicating we have taken a conservative approach of testing conditions that may be a little more challenging than reality.

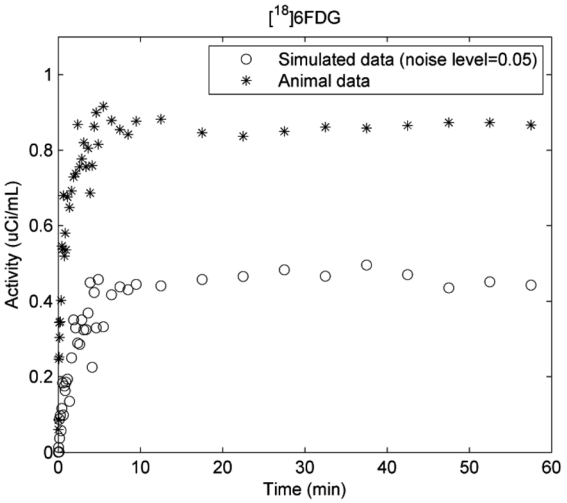

APPENDIX C: ADDITIONAL SIMULATION RESULTS

TABLE SI. Summary of parameter estimates for basal conditions.

Noise levels		0.01	0.05	0.1
Parameters	True	500 sets of estimates (mean ± SD)		
k_1 (mL/mL min^{-1})	0.04	0.04 ± 0.00	0.04 ± 0.00	0.04 ± 0.00
IS_g (mM)	5.10	5.10 ± 0.01	5.12 ± 0.04	5.13 ± 0.07
IC_g (mM)	0.05	0.06 ± 0.05	0.13 ± 0.16	0.16 ± 0.20
f_{IS} (unitless)	0.25	0.25 ± 0.00	0.25 ± 0.00	0.25 ± 0.01
V^G (mmol/min/mL tissue)	0.06	0.06 ± 0.00	0.06 ± 0.00	0.06 ± 0.00
V^H (mmol/min/mL tissue)	0.13	0.39 ± 0.82	0.48 ± 0.98	0.65 ± 1.20
CI (mmol/min/mL tissue)	0.0369	0.0370 ± 0.0005	0.0377 ± 0.0017	0.0377 ± 0.0028
CE (mmol/min/mL tissue)	0.0009	0.0009 ± 0.0008	0.0023 ± 0.0027	0.0028 ± 0.0033
PR (mmol/min/mL tissue)	0.0360	0.0360 ± 0.0004	0.0354 ± 0.0018	0.0349 ± 0.0027
k_2 (min^{-1})	0.16	0.16 ± 0.00	0.16 ± 0.01	0.16 ± 0.01
k_{3_6FDG} (min^{-1})	0.0101	0.0102 ± 0.0001	0.0104 ± 0.0001	0.0103 ± 0.0011
k_{4_6FDG}(min^{-1})	0.0082	0.0082 ± 0.0001	0.0081 ± 0.0002	0.0081 ± 0.0004
k_{3_2FDG}(min^{-1})	0.0127	0.0127 ± 0.0002	0.0130 ± 0.0007	0.0129 ± 0.0013
k_{4_2FDG}(min^{-1})	0.0102	0.0102 ± 0.0001	0.0102 ± 0.0003	0.0101 ± 0.0005
k_{5_2FDG}(min^{-1})	0.7341	2.79 ± 6.43	3.49 ± 7.68	4.83 ± 9.40

TABLE SII. Summary of parameter estimates for EH conditions.

Noise levels		0.01	0.05	0.1
Parameters	True	500 sets of estimates (mean ± SD)		
k_1 (mL/mL min^{-1})	0.044	0.04 ± 0.00	0.04 ± 0.00	0.05 ± 0.00
IS_g (mM)	3.00	3.00 ± 0.04	3.04 ± 0.13	3.08 ± 0.20
IC_g (mM)	0.13	0.14 ± 0.04	0.19 ± 0.15	0.22 ± 0.20
f_{IS} (unitless)	0.25	0.25 ± 0.00	0.24 ± 0.02	0.24 ± 0.02
V^G (mmol/min/mL tissue)	0.31	0.31 ± 0.00	0.32 ± 0.02	0.32 ± 0.03
V^H (mmol/min/mL tissue)	0.26	0.26 ± 0.06	1.93 ± 4.04	3.04 ± 5.07
CI (mmol/min/mL tissue)	0.1435	0.1441 ± 0.0029	0.1477 ± 0.0124	0.1511 ± 0.0166
CE (mmol/min/mL tissue)	0.0115	0.0123 ± 0.0032	0.0162 ± 0.0138	0.0198 ± 0.0183
PR (mmol/min/mL tissue)	0.1320	0.1380 ± 0.0005	0.1315 ± 0.0024	0.1313 ± 0.0183
k_2 (min^{-1})	0.176	0.177 ± 0.004	0.183 ± 0.020	0.019 ± 0.033
k_{3_6FDG} (min^{-1})	0.0670	0.0673 ± 0.0017	0.0699 ± 0.0077	0.0719 ± 0.0109
k_{4_6FDG}(min^{-1})	0.0399	0.0399 ± 0.0001	0.0399 ± 0.0004	0.0399 ± 0.0008
k_{3_2FDG}(min^{-1})	0.0837	0.0842 ± 0.0021	0.0874 ± 0.0096	0.0898 ± 0.0136
k_{4_2FDG}(min^{-1})	0.0499	0.0499 ± 0.0001	0.0499 ± 0.0005	0.0499 ± 0.0010
k_{5_2FDG}(min^{-1})	0.9977	1.0330 ± 0.4488	14.31 ± 32.14	23.08 ± 40.27

TABLE SIII. Summary of bias and precision for both basal and EH conditions at different noise levels.

500 sets of parameter estimates						
Conditions	Basal			EH		
Noise levels	0.01	0.05	0.1	0.01	0.05	0.1
Parameters	Error %(mean ± SD)					
k_1	0.27 ± 0.60	0.32 ± 2.81	0.30 ± 5.90	−0.02 ± 0.96	1.05 ± 4.48	2.79 ± 8.36
IS_g	0.05 ± 0.22	0.34 ± 0.86	0.57 ± 1.30	0.13 ± 1.04	1.24 ± 4.41	2.74 ± 6.81
IC_g	16 ± 90	163 ± 322	228 ± 391	6 ± 28	37 ± 114	66 ± 152
f_{IS}	0.03 ± 0.38	−0.43 ± 1.76	−0.07 ± 3.33	−0.28 ± 1.47	−2.05 ± 6.31	−3.34 ± 9.38
V^G	0.30 ± 1.20	2.03 ± 4.51	1.91 ± 7.59	0.29 ± 1.53	2.17 ± 6.45	3.67 ± 8.63
V^H	202 ± 632	271 ± 757	402 ± 926	1.63 ± 21.81	645 ± 1559	1082 ± 1956
CI	0.32 ± 1.26	2.17 ± 4.65	2.14 ± 7.63	0.36 ± 2.04	2.92 ± 8.62	5.27 ± 11.59
CE	16 ± 90	159 ± 312	219 ± 379	6 ± 28	40 ± 119	72 ± 159
PR	0.03 ± 1.22	−1.61 ± 4.97	−3.11 ± 7.40	−0.15 ± 0.38	−0.38 ± 1.84	−0.55 ± 3.26
k_2	0.31 ± 0.85	0.82 ± 4.01	0.59 ± 8.28	0.29 ± 2.34	3.85 ± 11.06	8.00 ± 18.53
k_{3_6FDG}	0.30 ± 1.47	2.36 ± 5.99	1.97 ± 10.60	0.54 ± 2.53	4.36 ± 11.50	7.30 ± 16.27
K_{4_6FDG}	0.07 ± 0.63	−0.37 ± 3.01	−1.26 ± 5.48	−0.03 ± 0.22	0.01 ± 1.06	−0.05 ± 2.09
K_{3_2FDG}	0.30 ± 1.47	2.36 ± 5.99	1.97 ± 10.60	0.54 ± 2.53	4.36 ± 11.50	7.30 ± 16.27
k_{4_2FDG}	0.07 ± 0.63	−0.37 ± 3.01	−1.26 ± 5.48	−0.03 ± 0.22	0.01 ± 1.06	−0.05 ± 2.09
k_{s_2FDG}	280 ± 875	375 ± 1046	557 ± 1281	3.54 ± 44.99	1334 ± 3221	2214 ± 4036

TABLE SIV. Summary of parameter estimates using different Michaelis constants for basal conditions.

			500 sets of parameter estimates (mean ± SD)			
Basal conditions	True	Assumed	k_1 (mL/mL min^{-1})	IS_g (mM)	IC_g (mM)	f_{IS}
True Michaelis constants			0.040 ± 0.001	5.12 ± 0.04	0.13 ± 0.16	0.25 ± 0.00
K_g^G(mM)	3.5	2.8	0.040 ± 0.001	4.94 ± 0.06	0.15 ± 0.17	0.25 ± 0.00
	3.5	4.5	0.040 ± 0.001	5.25 ± 0.03	0.12 ± 0.16	0.25 ± 0.00
K_g^H(mM)	0.13	0.104	0.040 ± 0.001	5.11 ± 0.04	0.12 ± 0.15	0.25 ± 0.00
	0.13	0.156	0.040 ± 0.001	5.12 ± 0.04	0.12 ± 0.16	0.25 ± 0.02
K_{6FDG}^G(mM)	10	8	0.040 ± 0.001	5.11 ± 0.03	0.01 ± 0.02	0.24 ± 0.00
	10	12	0.040 ± 0.001	5.15 ± 0.04	0.36 ± 0.16	0.25 ± 0.00
K_{2FDG}^G(mM)	8	6.4	0.040 ± 0.001	5.29 ± 0.03	0.37 ± 0.15	0.25 ± 0.00
	8	9.6	0.040 ± 0.001	4.96 ± 0.03	0.02 ± 0.04	0.24 ± 0.00
K_{2FDG}^H(mM)	0.17	0.136	0.040 ± 0.001	5.12 ± 0.05	0.12 ± 0.15	0.25 ± 0.00
	0.17	0.204	0.040 ± 0.001	5.12 ± 0.04	0.12 ± 0.15	0.25 ± 0.00

TABLE SV. Summary of parameter estimates using different Michaelis constants for EH conditions.

			500 sets of parameter estimates (mean ± SD)			
EH conditions	True	Assumed	k_1 (mL/mL min^{-1})	IS_g (mM)	IC_g (mM)	f_{IS}
True Michaelis constants			0.045 ± 0.002	3.04 ± 0.13	0.19 ± 0.15	0.24 ± 0.02
K_g^G(mM)	3.5	2.8	0.045 ± 0.002	2.77 ± 0.14	0.27 ± 0.14	0.24 ± 0.01
	3.5	4.5	0.044 ± 0.002	3.27 ± 0.10	0.10 ± 0.12	0.25 ± 0.01
K_g^H(mM)	0.13	0.104	0.045 ± 0.002	3.01 ± 0.11	0.16 ± 0.14	0.24 ± 0.02
	0.13	0.156	0.045 ± 0.002	3.07 ± 0.15	0.21 ± 0.17	0.25 ± 0.02
K_{6FDG}^G(mM)	10	8	0.046 ± 0.002	3.01 ± 0.08	0.01 ± 0.03	0.23 ± 0.01
	10	12	0.043 ± 0.002	3.06 ± 0.11	0.36 ± 0.13	0.26 ± 0.01
K_{2FDG}^G(mM)	8	6.4	0.043 ± 0.002	3.33 ± 0.08	0.41 ± 0.09	0.26 ± 0.01
	8	9.6	0.047 ± 0.002	2.77 ± 0.07	0.01 ± 0.03	0.23 ± 0.01
K_{2FDG}^H(mM)	0.17	0.136	0.045 ± 0.002	3.08 ± 0.16	0.22 ± 0.18	0.25 ± 0.02
	0.17	0.204	0.044 ± 0.002	3.01 ± 0.12	0.16 ± 0.14	0.25 ± 0.02

[a]Electronic mail: raymond.muzic@case.edu

[1]L. Sokoloff, M. Reivich, C. Kennedy, M. H. Des Rosiers, C. S. Patlak, K. D. Pettigrew, O. Sakurada,and M. Shinohara, "The [14C]deoxyglucose method for the measurement of local cerebral glucose utilization: theory, procedure, and normal values in the conscious and anesthetized albino rat," J. Neurochem. **28**, 897–916 (1977).

[2]M. E. Phelps, S. C. Huang, E. J. Hoffman, C. Selin, L. Sokoloff, and D. E. Kuhl, "Tomographic measurement of local cerebral glucose metabolic rate in humans with (F-18)2-fluoro-2-deoxy- D-glucose: Validation of method," Ann. Neurol. **6**, 371–388 (1979).

[3]A. Bertoldo, P. Peltoniemi, V. Oikonen, J. Knuuti, P. Nuutila, and C. Cobelli, "Kinetic modeling of [(18)F]FDG in skeletal muscle by PET: A four-compartment five-rate-constant model," Am. J. Physiol. Endocrinol. Metab. **281**, 524–536 (2001).

[4]A. Bertoldo, R. R. Pencek, K. Azuma, J. C. Price, C. Kelley, C. Cobelli, and D. E. Kelley, "Interactions between delivery, transport, and phosphorylation of glucose in governing uptake into human skeletal muscle," Diabetes **55**, 3028–3037 (2006).

[5]F. Schuier, F. Orzi, S. Suda, G. Lucignani, C. Kennedy, and L. Sokoloff, "Influence of plasma glucose concentration on lumped constant of the deoxyglucose method: Effects of hyperglycemia in the rat," J. Cereb. Blood. Flow. Metab. **10**, 765–773 (1990).

[6]S. Suda, M. Shinohara, M. Miyaoka, G. Lucignani, C. Kennedy, and L. Sokoloff, "The lumped constant of the deoxyglucose method in hypoglycemia: Effects of moderate hypoglycemia on local cerebral glucose utilization in the rat," J. Cereb. Blood. Flow. Metab. **10**, 499–509 (1990).

[7]B. R. Landau, C. L. Spring-Robinson, Jr. R. F. Muzic, N. Rachdaoui, D. Rubin, M. S. Berridge, W. C. Schumann, V. Chandramouli, T. S. Kern, and F. Ismail-Beigi, "6-Fluoro-6-deoxy-D-glucose as a tracer of glucose transport," Am. J. Physiol. Endocrinol. Metab. **293**, 237–245 (2007).

[8]J. A. Johnson and T. A. Wilson, "A model for capillary exchange," Am. J. Physiol. **210**, 1299–1303 (1966).

[9]E. M. Renkin, "Transport of potassium-42 from blood to tissue in isolated mammalian skeletal muscle," Am. J. Physiol. **197**, 1205–1210 (1959).

[10]M. Dixon and E. C. Webb, *Enzymes* (Academic, Inc., New York, 1979).

[11]L. P. Taylor and G. D. Holman, "Symmetrical kinetic parameters for 3-O-methyld-glucose transport in adipocytes in the presence and absence of insulin," Biochim. Biophys. Acta. **642**, 325–335 (1981).

[12]P. D. Crane, W. M. Pardridge, L. D. Braun, and W. H. Oldendorf, "Kinetics of transport and phosphorylation of 2-fluoro-2-deoxy-D-glucose in rat brain," J. Neurochem. **40**, 160–167 (1983).

[13]K. Mori and M. Maeda, "Use of [3H]methylglucose and [14C]iodoantipyrine to determine kinetic parameters of glucose transport in rat brain," Am. J. Physiol. **272**, 163–171 (1997).

[14]W. M. Pardridge and W. H. Oldendorf, "Kinetics of blood-brain transport of hexoses," Biochim. Biophys. Acta. **382**, 377–392 (1975).

[15]J. Cieslar, M. T. Huang, and G. P. Dobson, "Tissue spaces in rat heart, liver, and skeletal muscle in vivo," Am. J. Physiol. **275**, 1530–1536 (1998).

[16]C. Cobelli, D. Foster, and G. Toffolo, *Tracer Kinetics in Biomedical Research: From Data to Model* (Kluwer Academic/ Plenum, New York, 2001).

[17]R. F. Muzic, Jr. and S. Cornelius, "COMKAT: Compartment model kinetic analysis tool," J. Nucl. Med. **42**, 636–645 (2001).

[18]Y. H. Fang, P. Asthana, C. Salinas, H. M. Huang, and Jr. R. F. Muzic, "Integrated software environment based on COMKAT for analyzing tracer pharmacokinetics with molecular imaging," J. Nucl. Med. **51**, 77–84 (2010).

[19]Y. H. Fang and R. F. Muzic, Jr. "Spillover and partial-volume correction for image-derived input functions for small-animal 18F-FDG PET studies," J. Nucl. Med. **49**, 606–614 (2008).

[20]A. E. Halseth, D. P. Bracy, and D. H. Wasserman, "Functional limitations to glucose uptake in muscles comprised of different fiber types," Am. J. Physiol. Endocrinol. Metab. **280**, 994–999 (2001).

[21]M. Muzi, S. D. Freeman, R. C. Burrows, R. W. Wiseman, J. M. Link, K. A. Krohn, M. M. Graham, and A. M. Spence, "Kinetic characterization of hexokinase isoenzymes from glioma cells: implications for FDG imaging of human brain tumors," Nucl. Med. Biol. **28**, 107–116 (2001).

[22]C. L. Spring-Robinson, V. Chandramouli, W. C. Schumann, P. F. Faulhaber, Y. Wang, C. Wu, F. Ismail-Beigi, and Jr. R. F. Muzic, "Uptake of 18F-labeled 6-fluoro-6-deoxy-D-glucose by skeletal muscle is responsive to insulin stimulation," J. Nucl. Med. **50**, 912–919 (2009).

[23]W. C. Steven, S. H. Karen, J. B. Brad, D. C. Poole, and T. I. Musch, "Effects of Type II diabetes on exercising skeletal muscle blood flow in the rat," J. Appl. Physiol. **109**, 1347–1353 (2010).

[24]P. A. King, M. F. Hirshman, E. D Horton, and E. S. Horton, "Glucose transport in skeletal muscle membrane vesicles from control and exercised rats," Am. J. Physiol. **257**, C1128–C1134 (1989).

[25]C. Postic, A. Leturque, F. Rencurel, R. L. Printz, C. Forest, D. K. Granner, and J. Girard, "The effects of hyperinsulinemia and hyperglycemia on GLUT4 and hexokinase II mRNA and protein in rat skeletal muscle and adipose tissue," Diabetes **42**, 922–929 (1993).

[26]M. A. Vincent, D. Dawson, A. D. Clark, J. R. Lindner, S. Rattigan, M. G. Clark, and E. J. Barrett, "Skeletal muscle microvascular recruitment by physiological hyperinsulinemia precedes increases in total blood flow," Diabetes **51**, 42–48 (2002).

[27]S. Gudbjörnsdóttir, M. Sjöstrand, L. Strindberg, J. Wahren, and P. Lönnroth, "Direct measurements of the permeability surface area for insulin and glucose in human skeletal muscle," J. Clin. Endocrinol. Metab. **88**, 4559–4564 (2003).

[28]Jr. R. F. Muzic and B. T. Christian, "Evaluation of objective functions for estimation of kinetic parameters," Med. Phys. **33**, 342–353 (2006).

[29]T. F. Coleman and Y. Li, "An interior trust region approach for nonlinear minimization subject to bounds," SIAM. J. Optim. **6**, 418–445 (1996).

[30]S. C. Huang, M. E. Phelps, E. J. Hoffman, K. Sideris, C. J. Selin, and D. E. Kuhl, "Noninvasive determination of local cerebral metabolic rate of glucose in man," Am. J. Physiol. **238**, 69–82 (1980).

[31]H. E. Morgan, J. R. Neely, and Y. Kira, "Factors determining the utilization of glucose in isolated rat hearts," Basic. Res. Cardiol. **79**, 292–299 (1984).

[32]A. Behrooz and F. Ismail-Beigi, "Stimulation of Glucose Transport by Hypoxia: Signals and Mechanisms," News. Physiol. Sci. **14**, 105–110 (1999).

[33]E. Ferrannini, J. D. Smith, C. Cobelli, G. Toffolo, A. Pilo, and R. A. DeFronzo, "Effect of insulin on the distribution and disposition of glucose in man," J. Clin. Invest. **76**, 357–364 (1985).

[34]C. R. Park, D. Reinwein, M. J. Henderson, E. Cadenas, and H. E. Morgan, "The action of insulin on the transport of glucose through the cell membrane," Am. J. Med. **26**, 674–684 (1959).

[35]R. C. Bonadonna, S. Del Prato, M. P. Saccomani, E. Bonora, G. Gulli, E. Ferrannini, D. Bier, C. Cobelli, and R. A. DeFronzo, "Transmembrane glucose transport in skeletal muscle of patients with non-insulin- dependent diabetes," J. Clin. Invest. **92**, 486–494 (1993).

[36]R. C. Bonadonna, M. P. Saccomani, and C. Cobelli, "In vivo glucose transport in human skeletal muscle: tools, problems and perspectives," Baillieres Clin. Endocrinol. Metab. **7**, 929–960 (1993).

[37]J. M. Ng, D. E. Kelley, and B. H. Goodpaster, "Mechanisms of insulin resistance assessed by dynamic in-vivo positron emission tomography imaging," Curr. Opin. Clin. Nutr. Metab. Care **12**, 508–512 (2009).

[38]K. V. Williams, J. C. Price, and D. E. Kelley "Interactions of impaired glucose transport and phosphorylation in skeletal muscle insulin resistance: A dose-response assessment using positron emission tomography," Diabetes **50**, 2069–2079 (2001).

[39]M. Pendergrass, A. Bertoldo, R. Bonadonna, G. Nucci, L. Mandarino, C. Cobelli, and R. A. Defronzo, "Muscle glucose transport and phosphorylation in type 2 diabetic, obese nondiabetic, and genetically predisposed individuals," Am. J. Physiol. Endocrinol. Metab. **292**, 92–100 (2007).

[40]C. Cobelli, D. Foster, and G. Toffolo. Tracer Kinetics in Biomedical Research: From Data to Model. New York: Kluwer Academic/Plenum, 2001.